Molecular tension authenticates apoptotic cells being phagocytosed

Chanhyuk Min[1,2,3]†, Hyeokjin Cho[1,2]†, Jeongmin Yu[1,2]†, Byeongjin Moon[1], Jaeseon Jeon[1], Nafeesa Shahdab[1]‡, Hyunji Moon[1] , Susumin Yang[1], Juyeon Lee[1], Jaeseong Jin[4], Mingi Hong[1,2], Won-jin Chung[4], Jihwan Park[1], Gwangrog Lee[2,3]*, Daeho Park[1]*

[1]School of Life Sciences, Gwangju Institute of Science and Technology; Gwangju 61005, Korea

[2]Protein Engineering & Mechano-ImmunoTheraphy Laboratory, Korea Advanced Institute of Science and Technology; Daejeon 34141, Korea

[3]Department of Biological Sciences, Korea Advanced Institute of Science and Technology; Daejeon 34141, Korea

[4]Department of Chemistry, Gwangju Institute of Science and Technology; Gwangju 61005, Korea

†These authors contributed equally: Chanhyuk Min, Hyeokjin Cho, Jeongmin Yu

‡Current Affiliation: School of Health and Life Sciences, Teesside University; Middlesbrough, United Kingdom

*Correspondence and requests for materials should be addressed to:

G.L. (email: ifglee@kaist.ac.kr) or D.P. (email: daehopark@gist.ac.kr)

Abstract

Profound cytoskeletal reorganization and plasma membrane deformation in phagocytes is indispensable for phagocytosis of massive apoptotic cells, but whether these dynamics accompany a mechanical signal modulating signaling during efferocytosis remains largely unexplored. Here, we report that tension between phosphatidylserine (PS) and PS receptors (PSR) generated at the phagocytic synapse serves as a signal to determine whether PS-exposing cells should be phagocytosed. Mechanistically, increased membrane tension of phagocytes via Rac1-dependent actin polymerization and membrane stiffness of apoptotic cells caused tension between PS and PSRs, leading to phosphoinositide 3-kinase recruitment to PSRs, which resulted in Rac1 inactivation and myosin II phosphorylation required for phagocytic cup closure. Our observations imply that tension between PS and PSRs acts as a mechanical fail-safe to prevent removal of all PS-exposing cells for the integrity of efferocytosis.

One-Sentence Summary

Tension between phosphatidylserine and its receptors acts as a final decision-maker determining phagocytosis of apoptotic cells.

38 **Main Text**

39 Phagocytosis of apoptotic cells, called efferocytosis, differs from other types of phagocytosis in
40 terms of the endogeny and size of the targets. Specifically, this process removes endogenously
41 generated apoptotic cells that are as large as phagocytes (*1, 2*). Elaborately coordinated
42 signaling between two types of biochemical signals, called 'eat-me' and 'don't eat-me' signals,
43 enables phagocytes to remove such endogenous and massive targets. Phagocytes sense cells
44 to be phagocytosed through eat-me signals, of which phosphatidylserine (PS) is the most well-
45 known, and cells not to be phagocytosed through don't eat-me signals (*3-8*). Accordingly, when
46 eat-me signals are present and don't eat-me signals are nullified on the cell surface, phagocytes
47 are convinced that the cells are apoptotic cells that should be phagocytosed, and ultimately
48 efferocytosis may occur (*9, 10*). Furthermore, concerted signaling between these two signals
49 induces cytoskeletal rearrangement, which results in plasma membrane deformation, allowing
50 phagocytes to engulf the massive targets (*11-13*). Nevertheless, it has not been sufficiently
51 assessed whether the two signals are decisive for efferocytosis to occur. In particular, the
52 drastic plasma membrane deformation and cytoskeletal rearrangement in phagocytes may
53 induce a tensile force (tension) between molecules interacting intra- and intercellularly on the
54 plasma membrane (e.g., PS on apoptotic cells and its receptors (PSRs) on phagocytes). This
55 force may interconnect with the conventional signaling of efferocytosis. However, it remains
56 unclear whether such a force exists and, if so, what role it plays in efferocytosis. In this study,
57 we investigated the existence, generation, and role of tension between PS and PSRs (referred
58 to as tension of PS-PSRs) in efferocytosis using various approaches including surrogates of
59 apoptotic cells that can be used to adjust tension of PS-PSRs and time-lapse confocal
60 microscopy.

61 To investigate whether tension of PS-PSRs exists during and is required for
62 efferocytosis, we devised beads with PS connected via a tension gauge tether (*14*) (PS-TGT) as

63 surrogates of apoptotic cells. In PS-TGT beads, PS is covalently conjugated to the Cy3- or Cy5-
64 labeled upper strand of a double-stranded DNA tether that is immobilized on neutravidin beads
65 and the TGT ruptures at a critical force, termed tension tolerance (Fig. 1A). When J774A.1 cells,
66 a murine macrophage cell line, were incubated with PS-TGT beads, the cells engulfed beads
67 with a 56 pN tension tolerance TGT (PS-TGT^{56pN}) more efficiently than beads with a 12 pN
68 tension tolerance TGT (PS-TGT^{12pN}), as measured by the number of engulfed beads per
69 phagocyte and the percentage of phagocytes engulfing the beads (Fig. 1, B and C, and movie
70 S1). Other macrophages, including peritoneal macrophages, bone marrow-derived
71 macrophages, and RAW264.7 cells, also engulfed PS-TGT^{56pN} beads more efficiently than PS-
72 TGT^{12pN} beads (fig. S1, A to C). However, the superior engulfment of TGT^{56pN} beads relative to
73 TGT^{12pN} beads by macrophages was not observed when phosphatidylcholine (PC) was
74 conjugated to the TGT instead of PS (Fig. 1D). Notably, these results were not dependent on
75 the amount of TGT immobilized on the beads because PS-TGT^{56pN} beads were consistently
76 engulfed more efficiently than PS-TGT^{12pN} beads and engulfment of PC-TGT^{56pN} beads was still
77 comparable with that of PC-TGT^{12pN} beads when various amounts of the TGT were immobilized
78 on the beads (fig. S1D).

79 We then investigated whether the TGT is indeed ruptured during engulfment of PS-TGT
80 beads. Several observations indicated that PS-TGT^{12pN}, but not PS-TGT^{56pN}, was ruptured
81 during engulfment of the beads. First, the Cy5 mean fluorescence intensity (MFI) of non-
82 engulfing phagocytes was higher upon incubation with PS-TGT^{12pN} beads than upon incubation
83 with PS-TGT^{56pN} or control TGT beads (Fig. 1E), implying that the ruptured Cy5-labeled upper
84 strand of PS-TGT^{12pN} is present in non-engulfing phagocytes. Second, after macrophages were
85 incubated on a polyethylene glycol (PEG)-passivated glass plate on which PS-TGT was
86 immobilized via a biotin-neutravidin interaction (*15*), cell detachment from the plate was
87 evaluated. The cell number was comparable on the PS-TGT^{12pN} and PS-TGT^{56pN} plates after

88 incubation for 5 min. However, after incubation for 60 min, few cells were present on the PS-
89 TGT^{12pN} plate, whereas most cells remained attached to the PS-TGT^{56pN} plate (Fig. 1F). This
90 also implies that PS-TGT^{12pN}, but not PS-TGT^{56pN}, is ruptured because the cells were attached
91 to the plate only through PS-TGT (fig. S1E). Third, the loss of Cy5 fluorescence, indicative of
92 rupture of the Cy5-labeled upper strand of the TGT, was greater with PS-TGT^{12pN} than with PS-
93 TGT^{56pN} when macrophages were incubated on glass plates (Fig. 1G and fig. S1F). Collectively,
94 these data imply that the degree of rupture of the PS-TGT differs depending on tension
95 tolerance during engulfment of PS-TGT beads, indicating that tension is loaded between PS
96 and PSRs during and is essential for efferocytosis.

97 The rupture of PS-TGT^{12pN} may cause the ligand to separate from the target, preventing
98 further signaling and potentially leading to inefficient engulfment of the PS-TGT^{12pN} beads. To test
99 this, we designed hairpin PS-TGTs with variable loop sizes, created using DNA or PEG, that
100 prevent the ligand from separating from the phagocytic target even when TGT rupture occurs. In
101 this measurement, the upper and lower strands of 12 pN TGT were connected by loops made of
102 PEG or ssDNA, creating TGTs with various tensions depending on the length of the loop (Fig. 1H).
103 For the hairpin TGTs with ssDNA after rupture (Fig. 1I), they are subjected to minimal entropic
104 tension of ~2.3 and ~3.6 pN for the 16-bp- and 50-bp-ssDNA loops, respectively, based on the
105 length-dependent elasticity of ssDNA. The results showed that macrophages still engulfed the
106 hairpin PS-TGT^{12pN} beads with significantly lower efficiency than hairpin or normal PS-TGT^{56pN}
107 beads, and there were no differences between engulfment of normal PS-TGT^{12pN} and hairpin PS-
108 TGT^{12pN} beads. Nevertheless, in the case of the PEG loop (Fig. 1J), as the loop size increased,
109 engulfment decreased at both 12 pN and 56 pN, which is believed to be due to increased steric
110 hindrance as loop size increases. Regardless of the loop size and type, the engulfment of hairpin
111 PS-TGT^{12pN} beads remained less efficient compared to the engulfment of hairpin PS-TGT^{56pN}
112 beads (Fig. 1, I and J), implying that inefficient engulfment of PS-TGT^{12pN} beads is not due to the

113 termination of signaling caused by the disassembly of the ligand from the phagocytic target.

114 We next investigated how tension of PS-PSRs affects engulfment of PS-TGT beads. To
115 this end, we scrutinized the binding, internalization, and degradation steps of efferocytosis. The
116 numbers of PS-TGT^{12pN} and PS-TGT^{56pN} beads bound to macrophages were comparable when
117 cells were incubated with the beads at 4°C (fig. S2A). F-actin formation, which is required for
118 internalization of apoptotic cells during efferocytosis and was monitored by phalloidin staining,
119 was also comparable around PS-TGT^{12pN} and PS-TGT^{56pN} beads (fig. S2B). In addition, neither
120 the acidification of phagolysosomes nor the degradation of phagolysosomal cargos, as measured
121 by the change rates of the fluorescence intensities of pHrodo and Cy3, respectively, was altered
122 according to the tension tolerance of PS-TGT beads (fig. S2, C and D, and movies S2 and S3).
123 However, unexpectedly, time-lapse observation of F-actin using SiR-actin, a live F-actin labeling
124 probe, revealed that F-actin persisted longer around PS-TGT^{12pN} beads than around PS-TGT^{56pN}
125 beads (Fig. 2, A and D, and movie S4). Disassembly of F-actin is synchronized with phagocytic
126 cup closure during efferocytosis (*16, 17*); therefore, we next monitored phagocytic cup closure
127 depending on tension tolerance during engulfment of PS-TGT beads. Macrophages often failed
128 to close the phagocytic cup to completely engulf PS-TGT^{12pN} beads and consequently it took
129 longer to close the phagocytic cup for engulfment of PS-TGT^{12pN} beads than for engulfment of
130 PS-TGT^{56pN} beads (Fig. 2, C and D, and movie S5). These data imply that tension of PS-PSRs
131 affects efferocytosis by modulating phagocytic cup closure but not by modulating the binding
132 capacity, F-actin formation, or phagolysosomal function of phagocytes during efferocytosis.

133 We then investigated how tension of PS-PSRs modulates phagocytic cup closure
134 during engulfment of PS-TGT beads. Rac1 is involved in an early signaling pathway leading to
135 efferocytosis and its activity regulates F-actin dynamics (*11, 18*). In particular, spatiotemporal
136 regulation of Rac1 activity at the phagocytic cup is crucial for phagocytic cup formation and
137 closure (*16*). Therefore, we investigated whether the tension affects Rac1 activity. To this end,

138 we used Raichu-Rac1, a biosensor that monitors Rac1 activity via fluorescence resonance
139 energy transfer (FRET) (*19*). Macrophages expressing Raichu-Rac1 were incubated with PS-
140 TGT beads, and FRET was measured at the interface between macrophages and the beads
141 from 0° to 180° in a circular fashion as a function of time. Rac1 activation was initiated at the
142 junction of macrophages and the beads and proceeded along the tip of the phagocytic cup. At
143 0–10 min, Rac1 was activated with similar FRET levels in phagocytes incubated with PS-
144 TGT^{12pN} and PS-TGT^{56pN} beads. By contrast, at 10–20 min, Rac1 activation was instantly
145 followed by its inactivation at the phagocytic cup of phagocytes incubated with PS-TGT^{56pN}
146 beads, but not of phagocytes incubated with PS-TGT^{12pN} beads (Fig. 2, E and F, and movies S6
147 and S7). In addition, given that constitutively active Rac1 (Rac1(CA)) has been reported to
148 interfere with phagocytic cup closure and inhibit efferocytosis, Rac1(CA) can mitigate the effect
149 of tension of PS-PSRs on engulfment of PS-TGT^{56pN} beads. To test this, we overexpressed
150 Rac1(CA) in phagocytes and evaluated its effect. As expected, engulfment of PS-TGT^{56pN} by
151 phagocytes overexpressing Rac1(CA) was impeded in a manner dependent on the level of
152 Rac1(CA) expression (fig. S2, E and F). These data suggest that tension of PS-PSRs
153 orchestrates phagocytic cup closure via spatiotemporal inactivation of Rac1 during
154 efferocytosis.

155 Along with Rac1 inactivation, myosin II-mediated contraction is necessary for
156 phagocytic cup closure (*20*). To investigate whether the tension also affects myosin II activity,
157 we performed a frustrated phagocytosis assay that can quantitatively evaluate phagocytic cup
158 extension and contraction (*21*). Macrophages were incubated on PS-TGT-coated plates and
159 their extension and contraction were monitored. During the extension phase, cells spread
160 comparably on PS-TGT^{12pN} and PS-TGT^{56pN} plates. However, during the contraction phase,
161 phagocytes contracted more slowly on the PS-TGT^{12pN} plate than on the PS-TGT^{56pN} plate. In
162 addition, treatment of cells with blebbistatin, a myosin II inhibitor, drastically delayed the

163 contraction of phagocytes on the PS-TGT^{56pN} plate such that it was similar to that on the PS-
164 TGT^{12pN} plate (Fig. 2G and movies S8 to S10). Higher levels of myosin light chain (MLC)
165 phosphorylation were observed around PS-TGT^{56pN} beads and at the leading edge of cells on
166 the PS-TGT^{56pN} plate when macrophages were incubated with PS-TGT beads and on PS-TGT
167 plates, respectively (Fig. 2H, fig. S3, A to C, and movie S11). Overall, these data imply that
168 tension of PS-PSRs causes Rac1 inactivation at the phagocytic cup, leading to both myosin II-
169 mediated contraction and F-actin disassembly required for phagocytic cup closure.
170 Next, we investigated how tension of PS-PSRs modulates Rac1 activity.
171 Phosphoinositide 3-kinase (PI3K) recruits GTPase-activating proteins (GAPs) for Rac1 by
172 generating PIP_3 at the phagocytic cup during efferocytosis, leading to Rac1 inactivation and thus
173 phagocytic cup closure (*22*). Therefore, we reasoned that the tension can alter PI3K activity. To
174 test whether PI3K affects tension tolerance-dependent engulfment, macrophages were treated
175 with LY294002, a PI3K inhibitor, and engulfment of the beads was evaluated. The inhibitor
176 completely abrogated the superior engulfment of PS-TGT^{56pN} beads relative to PS-TGT^{12pN}
177 beads (Fig. 3A), suggesting that PI3K is involved in tension tolerance-dependent engulfment of
178 PS-TGT beads. To further understand the relationship between the tension and PI3K activity, we
179 used the GFP-tagged PH domain of Akt (PH-Akt-GFP) that binds to PIP_3, which represents
180 PI3K activity. When PH-Akt-GFP-expressing macrophages were incubated with PS-TGT beads,
181 the GFP signal was higher in phagocytic cups around PS-TGT^{56pN} beads than in phagocytic
182 cups around PS-TGT^{12pN} beads, and this difference was nullified in the presence of the PI3K
183 inhibitor (Fig. 3, B and C, and movies S12 to S14). This implies that tension of PS-PSRs
184 increases the activity of PI3K, leading to Rac1 inactivation in the phagocytic cup.
185 We then explored how the tension modulates PI3K activity. Given that PI3K associates
186 with some engulfment receptors (e.g., Tim-1 and Mertk) and all experiments in this study were
187 performed under serum-free conditions in which only direct PSRs could participate in

188 engulfment of the beads (*23-27*), we investigated whether PI3K associates with PSRs and, if so,
189 whether the association is affected by tension of PS-PSRs. PI3K robustly associated with Tim-4
190 among members of the Tim family and BAI1 (Fig. 3D and fig. 4, A and B). In addition, to confirm
191 the subcellular location of the association between Tim-4 and PI3K at the endogenous level, a
192 proximity ligation assay (PLA) was performed. As a result, in macrophages incubated with PS-
193 TGT^{12pN} beads, PLA signals were not confined to the phagocytic cup and were observed
194 ubiquitously. However, in macrophages incubated with PS-TGT^{56pN} beads, most signals were
195 observed around the phagocytic cup (Fig. 3, E and F). Collectively, these data imply that tension
196 of PS-PSRs increases the association of PI3K with PSRs, e.g., Tim-4, sequentially resulting in
197 Rac1 inactivation, F-actin disassembly, and myosin II-mediated contraction, which ultimately
198 causes phagocytic cup closure.
199 To investigate how tension is loaded on PS-PSRs, actin and myosin were examined
200 because they generate force in cells and are essential for phagocytic cup formation and closure
201 during efferocytosis (*20, 28*). In addition, F-actin disassembly and myosin II-mediated
202 contraction were modulated in a tension tolerance-dependent manner during engulfment of PS-
203 TGT beads (Fig. 2, A, B, G, and H). This suggests that tension of PS-PSRs at the phagocytic
204 cup during efferocytosis can be loaded by actin dynamics and/or myosin II-mediated
205 contraction. To test this possibility, cell detachment from PS-TGT plates was evaluated in the
206 presence or absence of cytochalasin D and blebbistatin, which are inhibitors of actin
207 polymerization and myosin II-mediated contraction, respectively. Cytochalasin D blocked
208 detachment of macrophages from the glass plate to which they were connected via PS-TGT^{12pN}
209 (Fig. 4, A and B) and loss of Cy5 signals in Cy5-labeled PS-TGT^{12pN}, but blebbistatin did not
210 (Fig. 4C and fig. S5A). These data imply that actin polymerization, rather than myosin II-
211 mediated contraction, is crucial for tension loading between PS and PSRs at the phagocytic
212 cup. In addition, the tension is not due to an allosteric effect of PSRs induced by PS binding

213 because cytochalasin D still allows PS to bind to its receptors (Fig. 4A).

214 Given that membrane tension increases during phagocytic cup formation driven by actin
215 polymerization (*29*), this membrane tension may play an important role in loading tension on
216 PS-PSRs. To validate this, we decreased the membrane tension of macrophages using
217 hypertonic solution (*30, 31*). Indeed, the more efficient engulfment of PS-TGT^{56pN} beads relative
218 to PS-TGT^{12pN} beads was abrogated by treating macrophages with hypertonic solution (Fig. 4D).
219 The treatment also reduced the Cy5 MFI of non-engulfing phagocytes upon incubation with PS-
220 TGT^{12pN} beads, but that of non-engulfing phagocytes upon incubation with PS-TGT^{56pN} beads
221 was unaltered (fig. S5B). Furthermore, treatment with hypertonic solution diminished the GFP
222 signal, representing PI3K activity, around PS-TGT^{56pN} beads in macrophages expressing PH-
223 Akt-GFP (Fig. 4, E and F, and movie S15). Consistently, when apoptotic cells were used instead
224 of PS-TGT beads to increase the physiological relevance, phagocytosis of apoptotic cells was
225 drastically impaired when macrophages were treated with hypertonic solution (Fig. 4G). Overall,
226 these data imply that an increase in the membrane tension of phagocytes is coupled with an
227 increase in tension or loading rate exerted on PS-PSRs during efferocytosis.

228 The membrane stiffness of apoptotic cells is increased (*32, 33*), which is expected to be
229 necessary for loading tension on PS-PSRs during efferocytosis. To apply tension of PS-PSRs,
230 PS on the surface of apoptotic cells must be pulled by PSRs on phagocytes. In this situation,
231 the membrane stiffness of apoptotic cells may be crucial to reach a certain level of tension
232 generated by the pulling of PSRs within the limited phagocytic synaptic space. To validate this,
233 we altered the membrane stiffness of apoptotic cells using cytochalasin D, which decreases
234 membrane stiffness (*33*), and performed an efferocytosis assay. Treatment of apoptotic cells
235 with cytochalasin D substantially impeded efferocytosis *in vitro* and *in vivo* (Fig. 4, H and I).
236 Notably, the conditioned medium of apoptotic cells treated with cytochalasin D did not affect
237 efferocytosis, demonstrating that the direct effect of cytochalasin D released from apoptotic cells

238 on phagocytes was minimal (fig. S5C). In addition, cytochalasin D did not alter the status of
239 apoptotic cells (fig. S5D). These data imply that increased membrane stiffness in apoptotic cells
240 also contributes to tension generation between PS and PSRs during efferocytosis.

241 PS is exposed not only on apoptotic cells but also on some live cells, but only apoptotic
242 cells are phagocytosed (*9, 34-36*). In general, this is thought to be due to don't eat-me signals
243 such as CD47 on live cells (*10*). In addition to these signals, our observations strongly suggest
244 that tension of PS-PSRs is another decisive signal for efferocytosis. To investigate this, we
245 generated PS-exposing Jurkat cells using A23187, a calcium ionophore that stimulates PS
246 exposure on the cell surface without inducing apoptosis (fig. S5, E and F), and artificially
247 increased the membrane stiffness of Jurkat cells by depleting cholesterol using methyl-β-
248 cyclodextrin (MβCD) (*37, 38*). Macrophages efficiently engulfed Jurkat cells treated with both
249 A23187 and MβCD, but engulfment of Jurkat cells treated with A23187 or MβCD alone was
250 minimally increased compared with that of control Jurkat cells (Fig. 4J). To further validate the
251 physiological relevance of these findings, we used platelets, which expose PS on their surface
252 when they are activated for blood coagulation (fig. S5G) (*39, 40*). Engulfment of activated
253 platelets by macrophages was indistinguishable from that of non-activated platelets, but
254 activated platelets treated with MβCD were efficiently engulfed (Fig. 4K). Taken together, these
255 data suggest that tension of PS-PSRs, mediated by both increased membrane tension at the
256 phagocytic cup in phagocytes and membrane stiffness in apoptotic cells, acts as a checkpoint to
257 determine whether a PS-exposing cell should be phagocytosed and this tension is thus
258 essential for completion of efferocytosis.

259 In sum, we report that efferocytosis, a type of phagocytosis, is a novel example of a
260 process mediated by chemo-mechanical pathways. Upon binding between PS and PSRs, Rac1
261 is activated, resulting in actin polymerization to form the phagocytic cup around apoptotic cells
262 and thus increasing membrane tension concomitant with tension of PS-PSRs at the phagocytic

263 cup. When the tension reaches a substantial level (e.g., 56 pN), PI3K is recruited to PSRs at the
264 phagocytic cup, which results in Rac1 inactivation, leading to F-actin disassembly and myosin II-
265 mediated contraction required for phagocytic cup closure. Ultimately, tension of PS-PSRs must
266 be generated to successfully complete phagocytosis of apoptotic cells (fig. S6A).

267 Our findings provide insights into how chemical and mechanical signals generated
268 during phagocytosis of PS-exposing cells are delicately coordinated to enhance the integrity of
269 efferocytosis without errors. More specifically, biochemical signaling of efferocytosis initiated by
270 binding of PS to PSRs is converted into a mechanical signal (i.e., tension of PS-PSRs). The
271 tension is eventually converted back into a biochemical signal that determines whether PS-
272 exposing cells being engulfed are completely phagocytosed (fig. S6B). By generating a
273 mechanical signal during phagocytosis of PS-exposing cells, phagocytes can avoid removing all
274 PS-exposing cells and precisely remove cells to be cleared, e.g., apoptotic cells. Indeed, many
275 live cells expose PS on their surfaces including some cancer cells (*34-36, 41-44*). Cancer
276 immunotherapy based on innate immunity has recently attracted much attention (*45*). Cancer
277 cells may evade phagocytosis by immune cells via nullifying this type of mechanical signal as a
278 checkpoint during phagocytosis. It would be interesting to investigate the correlation of cancer
279 cell phagocytosis with tension between a ligand on cancer cells and its corresponding receptor
280 on immune cells, which may provide insight to develop cancer immunotherapy.

281
282

283 **References and Notes**

284 1. S. Arandjelovic, K. S. Ravichandran, Phagocytosis of apoptotic cells in homeostasis. *Nat*
285 *Immunol* **16**, 907-917 (2015).
286 2. A. C. Doran, A. Yurdagul, Jr., I. Tabas, Efferocytosis in health and disease. *Nat Rev*
287 *Immunol* **20**, 254-267 (2020).
288 3. V. A. Fadok, D. L. Bratton, S. C. Frasch, M. L. Warner, P. M. Henson, The role of
289 phosphatidylserine in recognition of apoptotic cells by phagocytes. *Cell Death Differ* **5**,
290 551-562 (1998).
291 4. V. A. Fadok *et al.*, Exposure of phosphatidylserine on the surface of apoptotic
292 lymphocytes triggers specific recognition and removal by macrophages. *J Immunol* **148**,
293 2207-2216 (1992).
294 5. P. A. Oldenborg *et al.*, Role of CD47 as a marker of self on red blood cells. *Science* **288**,
295 2051-2054 (2000).
296 6. A. A. Barkal *et al.*, CD24 signalling through macrophage Siglec-10 is a target for cancer
297 immunotherapy. *Nature* **572**, 392-396 (2019).
298 7. S. Brown *et al.*, Apoptosis disables CD31-mediated cell detachment from phagocytes
299 promoting binding and engulfment. *Nature* **418**, 200-203 (2002).
300 8. A. A. Barkal *et al.*, Engagement of MHC class I by the inhibitory receptor LILRB1
301 suppresses macrophages and is a target of cancer immunotherapy. *Nat Immunol* **19**, 76-
302 84 (2018).
303 9. K. Segawa, J. Suzuki, S. Nagata, Constitutive exposure of phosphatidylserine on viable
304 cells. *Proc Natl Acad Sci U S A* **108**, 19246-19251 (2011).
305 10. S. Jaiswal *et al.*, CD47 is upregulated on circulating hematopoietic stem cells and
306 leukemia cells to avoid phagocytosis. *Cell* **138**, 271-285 (2009).
307 11. J. M. Kinchen, K. S. Ravichandran, Journey to the grave: signaling events regulating

308 removal of apoptotic cells. *J Cell Sci* **120**, 2143-2149 (2007).
309 12. R. K. Tsai, D. E. Discher, Inhibition of "self" engulfment through deactivation of myosin-II
310 at the phagocytic synapse between human cells. *J Cell Biol* **180**, 989-1003 (2008).
311 13. S. Mylvaganam, S. A. Freeman, S. Grinstein, The cytoskeleton in phagocytosis and
312 macropinocytosis. *Curr Biol* **31**, R619-R632 (2021).
313 14. X. Wang, T. Ha, Defining single molecular forces required to activate integrin and notch
314 signaling. *Science* **340**, 991-994 (2013).
315 15. R. Roy, S. Hohng, T. Ha, A practical guide to single-molecule FRET. *Nat Methods* **5**, 507-
316 516 (2008).
317 16. M. Nakaya, M. Kitano, M. Matsuda, S. Nagata, Spatiotemporal activation of Rac1 for
318 engulfment of apoptotic cells. *Proc Natl Acad Sci U S A* **105**, 9198-9203 (2008).
319 17. H. Moon *et al.*, Crbn modulates calcium influx by regulating Orai1 during efferocytosis.
320 *Nat Commun* **11**, 5489 (2020).
321 18. M. R. Elliott, K. M. Koster, P. S. Murphy, Efferocytosis Signaling in the Regulation of
322 Macrophage Inflammatory Responses. *J Immunol* **198**, 1387-1394 (2017).
323 19. R. E. Itoh *et al.*, Activation of rac and cdc42 video imaged by fluorescent resonance
324 energy transfer-based single-molecule probes in the membrane of living cells. *Mol Cell*
325 *Biol* **22**, 6582-6591 (2002).
326 20. Y. Ikeda *et al.*, Rac1 switching at the right time and location is essential for Fcgamma
327 receptor-mediated phagosome formation. *J Cell Sci* **130**, 2530-2540 (2017).
328 21. D. T. Kovari *et al.*, Frustrated Phagocytic Spreading of J774A-1 Macrophages Ends in
329 Myosin II-Dependent Contraction. *Biophys J* **111**, 2698-2710 (2016).
330 22. D. Schlam *et al.*, Phosphoinositide 3-kinase enables phagocytosis of large particles by
331 terminating actin assembly through Rac/Cdc42 GTPase-activating proteins. *Nat*
332 *Commun* **6**, 8623 (2015).

333 23. P. Sen *et al.*, Apoptotic cells induce Mer tyrosine kinase-dependent blockade of NF-
334 kappaB activation in dendritic cells. *Blood* **109**, 653-660 (2007).
335 24. A. J. de Souza *et al.*, T cell Ig and mucin domain-1-mediated T cell activation requires
336 recruitment and activation of phosphoinositide 3-kinase. *J Immunol* **180**, 6518-6526
337 (2008).
338 25. G. X. Ruan, A. Kazlauskas, Axl is essential for VEGF-A-dependent activation of
339 PI3K/Akt. *EMBO J* **31**, 1692-1703 (2012).
340 26. M. Miyanishi *et al.*, Identification of Tim4 as a phosphatidylserine receptor. *Nature* **450**,
341 435-439 (2007).
342 27. D. Park *et al.*, BAI1 is an engulfment receptor for apoptotic cells upstream of the
343 ELMO/Dock180/Rac module. *Nature* **450**, 430-434 (2007).
344 28. K. Carvalho *et al.*, Actin polymerization or myosin contraction: two ways to build up
345 cortical tension for symmetry breaking. *Philos Trans R Soc Lond B Biol Sci* **368**,
346 20130005 (2013).
347 29. V. Jaumouille, C. M. Waterman, Physical Constraints and Forces Involved in
348 Phagocytosis. *Front Immunol* **11**, 1097 (2020).
349 30. A. R. Houk *et al.*, Membrane tension maintains cell polarity by confining signals to the
350 leading edge during neutrophil migration. *Cell* **148**, 175-188 (2012).
351 31. T. A. Masters, B. Pontes, V. Viasnoff, Y. Li, N. C. Gauthier, Plasma membrane tension
352 orchestrates membrane trafficking, cytoskeletal remodeling, and biochemical signaling
353 during phagocytosis. *Proc Natl Acad Sci U S A* **110**, 11875-11880 (2013).
354 32. N. I. Nikolaev, T. Muller, D. J. Williams, Y. Liu, Changes in the stiffness of human
355 mesenchymal stem cells with the progress of cell death as measured by atomic force
356 microscopy. *J Biomech* **47**, 625-630 (2014).
357 33. W. A. Lam, M. J. Rosenbluth, D. A. Fletcher, Chemotherapy exposure increases

358 leukemia cell stiffness. *Blood* **109**, 3505-3508 (2007).
359 34. J. I. Elliott *et al.*, Membrane phosphatidylserine distribution as a non-apoptotic signalling
360 mechanism in lymphocytes. *Nat Cell Biol* **7**, 808-816 (2005).
361 35. S. Riedl *et al.*, In search of a novel target - phosphatidylserine exposed by non-apoptotic
362 tumor cells and metastases of malignancies with poor treatment efficacy. *Biochim*
363 *Biophys Acta* **1808**, 2638-2645 (2011).
364 36. S. M. Qadri, R. Bissinger, Z. Solh, P. A. Oldenborg, Eryptosis in health and disease: A
365 paradigm shift towards understanding the (patho)physiological implications of
366 programmed cell death of erythrocytes. *Blood Rev* **31**, 349-361 (2017).
367 37. J. Suzuki, M. Umeda, P. J. Sims, S. Nagata, Calcium-dependent phospholipid
368 scrambling by TMEM16F. *Nature* **468**, 834-838 (2010).
369 38. A. Biswas, P. Kashyap, S. Datta, T. Sengupta, B. Sinha, Cholesterol Depletion by
370 MbetaCD Enhances Cell Membrane Tension and Its Variations-Reducing Integrity.
371 *Biophys J* **116**, 1456-1468 (2019).
372 39. S. M. Schoenwaelder *et al.*, Two distinct pathways regulate platelet phosphatidylserine
373 exposure and procoagulant function. *Blood* **114**, 663-666 (2009).
374 40. B. R. Lentz, Exposure of platelet membrane phosphatidylserine regulates blood
375 coagulation. *Prog Lipid Res* **42**, 423-438 (2003).
376 41. K. Fischer *et al.*, Antigen recognition induces phosphatidylserine exposure on the cell
377 surface of human CD8+ T cells. *Blood* **108**, 4094-4101 (2006).
378 42. J. I. Elliott *et al.*, Phosphatidylserine exposure in B lymphocytes: a role for lipid packing.
379 *Blood* **108**, 1611-1617 (2006).
380 43. K. J. de Vries, T. Wiedmer, P. J. Sims, B. M. Gadella, Caspase-independent exposure of
381 aminophospholipids and tyrosine phosphorylation in bicarbonate responsive human
382 sperm cells. *Biol Reprod* **68**, 2122-2134 (2003).

383 44. J. H. Stafford, P. E. Thorpe, Increased exposure of phosphatidylethanolamine on the
384 surface of tumor vascular endothelium. *Neoplasia* **13**, 299-308 (2011).
385 45. M. Feng *et al.*, Phagocytosis checkpoints as new targets for cancer immunotherapy. *Nat*
386 *Rev Cancer* **19**, 568-586 (2019).

387

388 **Acknowledgments**
389 We thank Michiyuki Matsuda (Kyoto University) and Jihye Seong (Korea Institute of Science
390 and Technology) for kindly providing the plasmids of Raichu-Rac1 and PH-Akt-GFP,
391 respectively.

392

393 **Funding**
394 This work was supported by the National Research Foundation of Korea funded by the Korea
395 government (MSIP) (2022R1A2C1008334 and 2022R1A4A2000790) and by GIST research
396 Institute (GRI) IIBR.

397

398 **Author contributions**
399 Conceptualization, G.L. and D.P.; Methodology, C.M., H.C, J.Y., B.M., J.J., N.S., H.M., S.Y., J.L.,
400 and M.H.; Formal analysis, C.M., H.C, J.Y., P.J., G.L., and D.P.; Resources, J.J. and W.-J.C.;
401 Writing, C.M., H.C, J.Y., G.L., and D.P.; Funding acquisition, G.L. and D.P.

402

403 **Competing interests**
404 The authors declare no competing interests.

405

406 **Data and materials availability**
407 Data from this study are available within the main text and the supplementary materials or from

408 the corresponding authors (G.L. and D.P.) upon reasonable request.

409

410 **Supplementary Materials**

411 Materials and Methods

412 Supplementary Text (Uncropped blots of western blot panels, Gating strategies used for flow

413 cytometry analysis, Movie legends, Synthesis of 18:1-12:0(maleimide) phosphatidylcholine)

414 Figs. S1 to S6

415 Movies S1 to S15

416

417

Figure 1

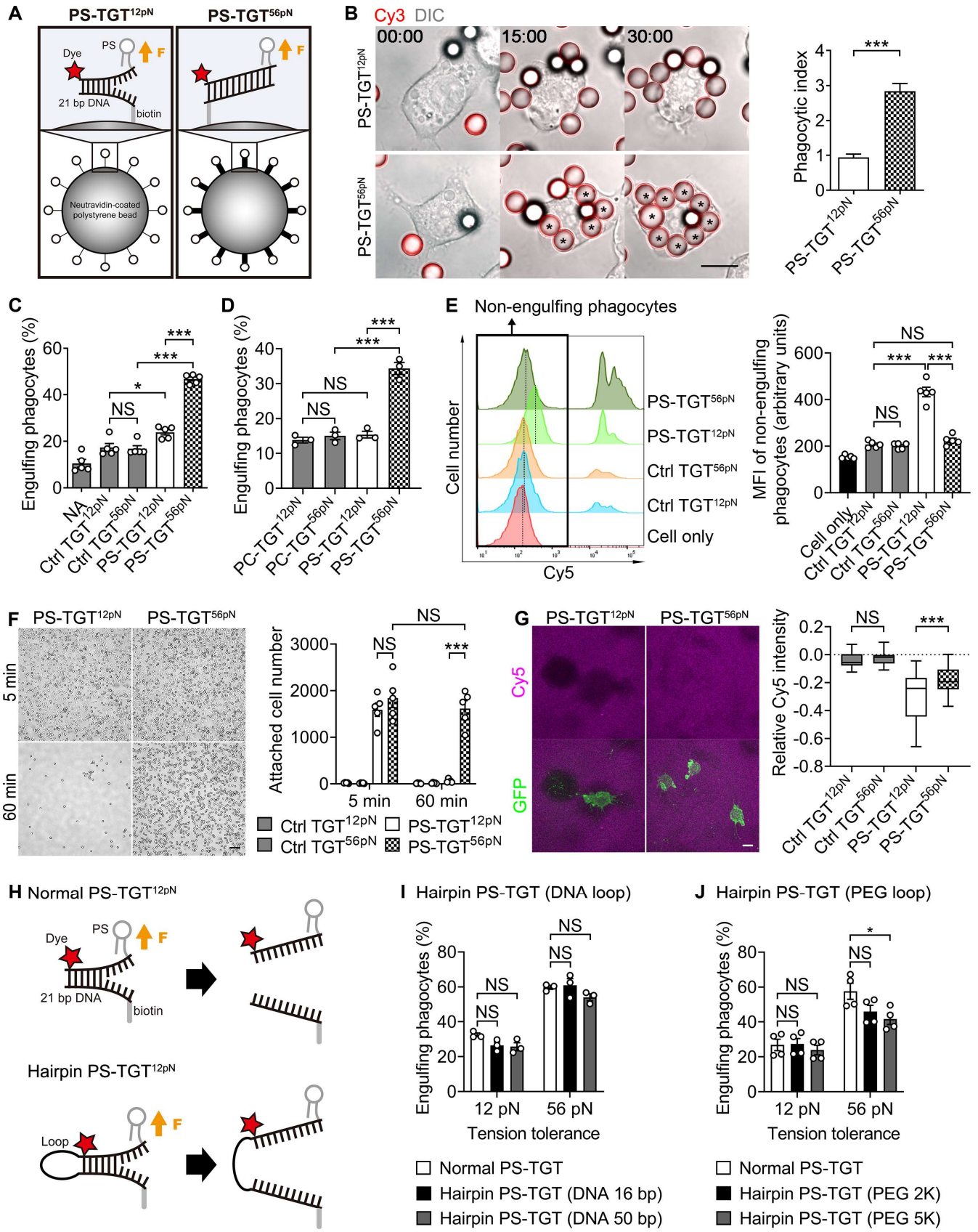
A
PS-TGT12pN
PS-TGT56pN
Dye
PS
F
21 bp DNA
biotin
Neutravidin-coated polystyrene bead
B
Cy3 DIC
00:00
15:00
30:00
PS-TGT12pN
PS-TGT56pN
Phagocytic index
***
C
Engulfing phagocytes (%)
NA
Ctrl TGT12pN
Ctrl TGT56pN
PS-TGT12pN
PS-TGT56pN
D
PC-TGT12pN
PC-TGT56pN
E
Non-engulfing phagocytes
Cell number
Cy5
Cell only
MFI of non-engulfing phagocytes (arbitrary units)
F
5 min
60 min
Attached cell number
Ctrl TGT12pN
Ctrl TGT56pN
PS-TGT12pN
PS-TGT56pN
G
Cy5
GFP
Relative Cy5 intensity
H Normal PS-TGT12pN
Hairpin PS-TGT12pN
Loop
I Hairpin PS-TGT (DNA loop)
12 pN
56 pN
Tension tolerance
Normal PS-TGT
Hairpin PS-TGT (DNA 16 bp)
Hairpin PS-TGT (DNA 50 bp)
J Hairpin PS-TGT (PEG loop)
Hairpin PS-TGT (PEG 2K)
Hairpin PS-TGT (PEG 5K)

418 **Fig. 1. Tension-dependent engulfment of PS-TGT beads.**

419 (**A**) Schematic diagram of PS-TGT beads. PS and biotin were conjugated to the Cy3- or Cy5-
420 labeled upper strand and the lower strand of 21 bp DNA, respectively, which was immobilized
421 on neutravidin-coated polystyrene beads via a neutravidin-biotin linker. Yellow arrows indicate
422 the direction of force (F). (**B**) J774A.1 cells incubated with Cy3-labeled PS-TGT^{12pN} or PS-
423 TGT^{56pN} beads for 30 min were observed by time-lapse confocal microscopy (left) and engulfed
424 beads were counted (right). Asterisks indicate ingested beads. Scale bar, 10 μm. Data are mean
425 ± s.e.m. from n=165 cells for PS-TGT^{12pN} and n=124 cells for PS-TGT^{56pN}. ***$P < 0.001$; two-
426 tailed unpaired Student's *t* test. (**C** and **D**) J774A.1 cells were incubated with the indicated
427 beads for 10 min and analyzed by flow cytometry. Ctrl, control; NA, neutravidin bead. Data are
428 mean ± s.e.m. from n=5 (C) and n=3 (D) independent experiments. *$P < 0.05$; ***$P < 0.001$; NS,
429 not significant; one-way ANOVA. (**E**) J774A.1 cells incubated with the indicated beads for 10
430 min were analyzed by flow cytometry. Representative histograms of phagocytes (left) and MFIs
431 of non-engulfing phagocytes (right) are shown. The box and dotted lines in the histograms
432 indicate non-engulfing phagocytes and the peak of the fluorescence intensity of non-engulfing
433 phagocytes, respectively. Data are mean ± s.e.m. from n=5 independent experiments.
434 ***$P < 0.001$; NS, not significant; one-way ANOVA. (**F**) J774A.1 cells were incubated on PS-TGT
435 plates, on which the indicated PS-TGTs were immobilized, for 5 min, washed, further incubated
436 for 60 min, and washed to remove detached cells. Scale bar, 200 μm. Data are mean ± s.e.m.
437 from n=5 independent experiments. ***$P < 0.001$; NS, not significant; two-way ANOVA. (**G**)
438 J774A.1 cells stably expressing membrane-targeted GFP (GFP-CAAX) were incubated on PS-
439 TGT plates, on which a mixture of the indicated Cy5-labeled PS-TGTs and Cy3-labeled PS-
440 TGT^{56pN} was immobilized, for 60 min and observed by confocal microscopy. Relative Cy5
441 intensities were calculated. The intensity of Cy5 in the area where cells were absent was set to
442 0. Scale bar, 10 μm. Data are represented in the box-and-whisker plot. n=26 cells for Ctrl

443 TGT^{12pN}, n=30 cells for Ctrl TGT^{56pN}, n=29 cells for PS-TGT^{12pN}, and n=49 cells for PS-TGT^{56pN}.
444 ***P < 0.001; NS, not significant; one-way ANOVA. (**H**) Schematic diagram of normal PS-
445 TGT^{12pN} (top) and hairpin PS-TGT^{12pN} (bottom). The upper and lower strands of hairpin PS-
446 TGT^{12pN} were connected by PEG or DNA loops. Yellow arrows indicate the direction of force (F).
447 (**I** and **J**) J774A.1 cells were incubated with the indicated beads for 15 min. Percentage of
448 engulfing phagocytes were measured by flow cytometry. Data are mean ± s.e.m. from n=3
449 independent experiments for (I), n=4 independent experiments for (J). *P < 0.05; NS, not
450 significant; two-way ANOVA.
451
452

Figure 2

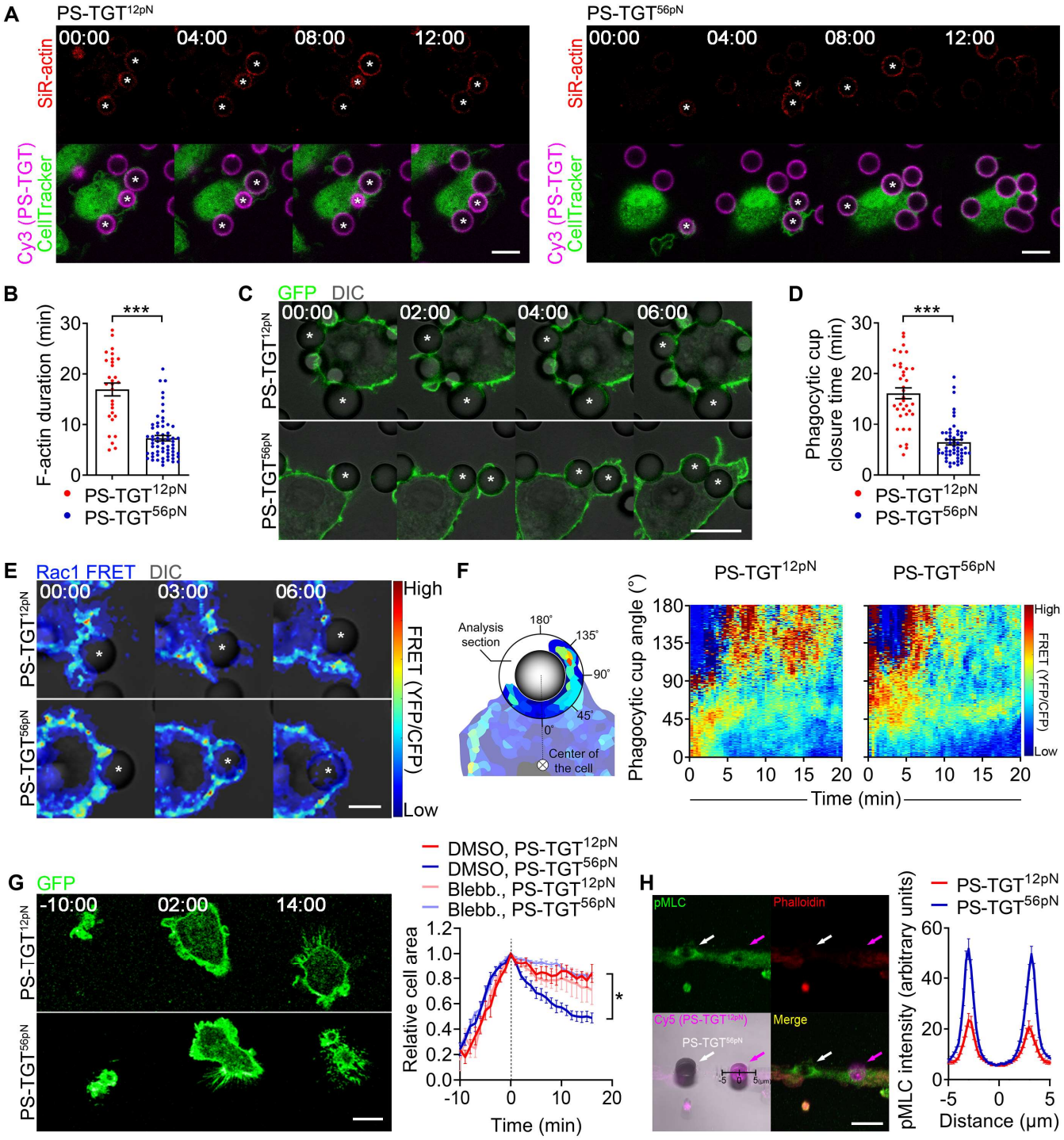
A
PS-TGT12pN
PS-TGT56pN
SiR-actin
Cy3 (PS-TGT)
CellTracker
00:00
04:00
08:00
12:00
B
F-actin duration (min)
***
PS-TGT12pN
PS-TGT56pN
C
GFP DIC
00:00
02:00
04:00
06:00
D
Phagocytic cup closure time (min)
E
Rac1 FRET DIC
03:00
06:00
High
Low
FRET (YFP/CFP)
F
Analysis section
180°
135°
90°
45°
0°
Center of the cell
Phagocytic cup angle (°)
Time (min)
G
GFP
-10:00
02:00
14:00
DMSO, PS-TGT12pN
DMSO, PS-TGT56pN
Blebb., PS-TGT12pN
Blebb., PS-TGT56pN
Relative cell area
H
pMLC
Phalloidin
Cy5 (PS-TGT12pN)
Merge
pMLC intensity (arbitrary units)
Distance (μm)

453 **Fig. 2. The tension affects engulfment of PS-TGT beads through Rac1.**

454 (**A** and **B**) J774A.1 cells stained with SiR-actin were incubated with Cy3-labeled PS-TGT beads
455 for 30 min and observed by time-lapse confocal microscopy (A). The duration of F-actin labeling
456 was measured (B). Asterisks indicate PS-TGT beads with SiR-actin signals. Scale bar, 10 μm.
457 Data are mean ± s.e.m. from n=29 beads for PS-TGT^{12pN} and n=62 beads for PS-TGT^{56pN}.
458 ***P < 0.001; two-tailed unpaired Student's *t* test. (**C** and **D**) J774A.1 cells stably expressing
459 membrane-targeted GFP were incubated with Cy3-labeled PS-TGT beads for 30 min and
460 observed by time-lapse confocal microscopy (C). Asterisks indicate beads with extended
461 phagocytic cups. The amount of time required for phagocytic cup closure was measured (D).
462 Scale bar, 10 μm. Data are mean ± s.e.m. from n=36 beads for PS-TGT^{12pN} and n=54 beads for
463 PS-TGT^{56pN}. ***P < 0.001; two-tailed unpaired Student's *t* test. (**E** and **F**) J774A.1 cells stably
464 expressing Raichu-Rac1 were incubated with PS-TGT beads for 30 min and observed by time-
465 lapse confocal microscopy (E). Asterisks indicate beads with extended phagocytic cups. Rac1
466 activity in phagocytic cups around the beads was calculated by YFP/CFP ratio FRET. Scale bar,
467 5 μm. Schematic diagram depicting the analysis of Rac1 FRET according to the phagocytic cup
468 position (F, left). Rac1 activity was measured at the phagocytic cup around the beads (F, right).
469 n=33 beads for PS-TGT^{12pN} and n=23 beads for PS-TGT^{56pN}. (**G**) J774A.1 cells stably
470 expressing membrane-targeted GFP were incubated on the indicated PS-TGT plates with or
471 without blebbistatin (10 μM) and observed by time-lapse confocal microscopy. When the cells
472 were maximally expanded, the time and relative area were set to 0 min and 1, respectively. The
473 areas of cells on the plates were normalized to the maximum area. Scale bar, 10 μm. Blebb,
474 blebbistatin. Data are mean ± s.e.m. from n=8 cells for PS-TGT^{12pN} (DMSO), n=11 cells for PS-
475 TGT^{56pN} (DMSO), n=16 cells for PS-TGT^{12pN} (Blebb.), and n=8 cells for PS-TGT^{56pN} (Blebb.).
476 Statistical analysis was performed between the end points of PS-TGT^{12pN} (DMSO) and PS-
477 TGT^{56pN} (DMSO). *P < 0.05; one-way ANOVA. (**H**) J774A.1 cells were incubated with both Cy5-

478 labeled PS-TGT^{12pN} and unlabeled PS-TGT^{56pN} beads for 10 min, stained with an anti-phospho-
479 MLC antibody and Alexa Fluor 594-conjugated phalloidin, and observed by confocal
480 microscopy. Magenta and white arrows indicate PS-TGT^{12pN} and PS-TGT^{56pN} beads,
481 respectively. The intensities of phosphorylated MLC (pMLC) staining were quantified across the
482 phagocytic cups. Scale bar, 10 μm. Data are mean ± s.e.m. from n=26 beads for PS-TGT^{12pN}
483 and PS-TGT^{56pN}.
484
485

Figure 3

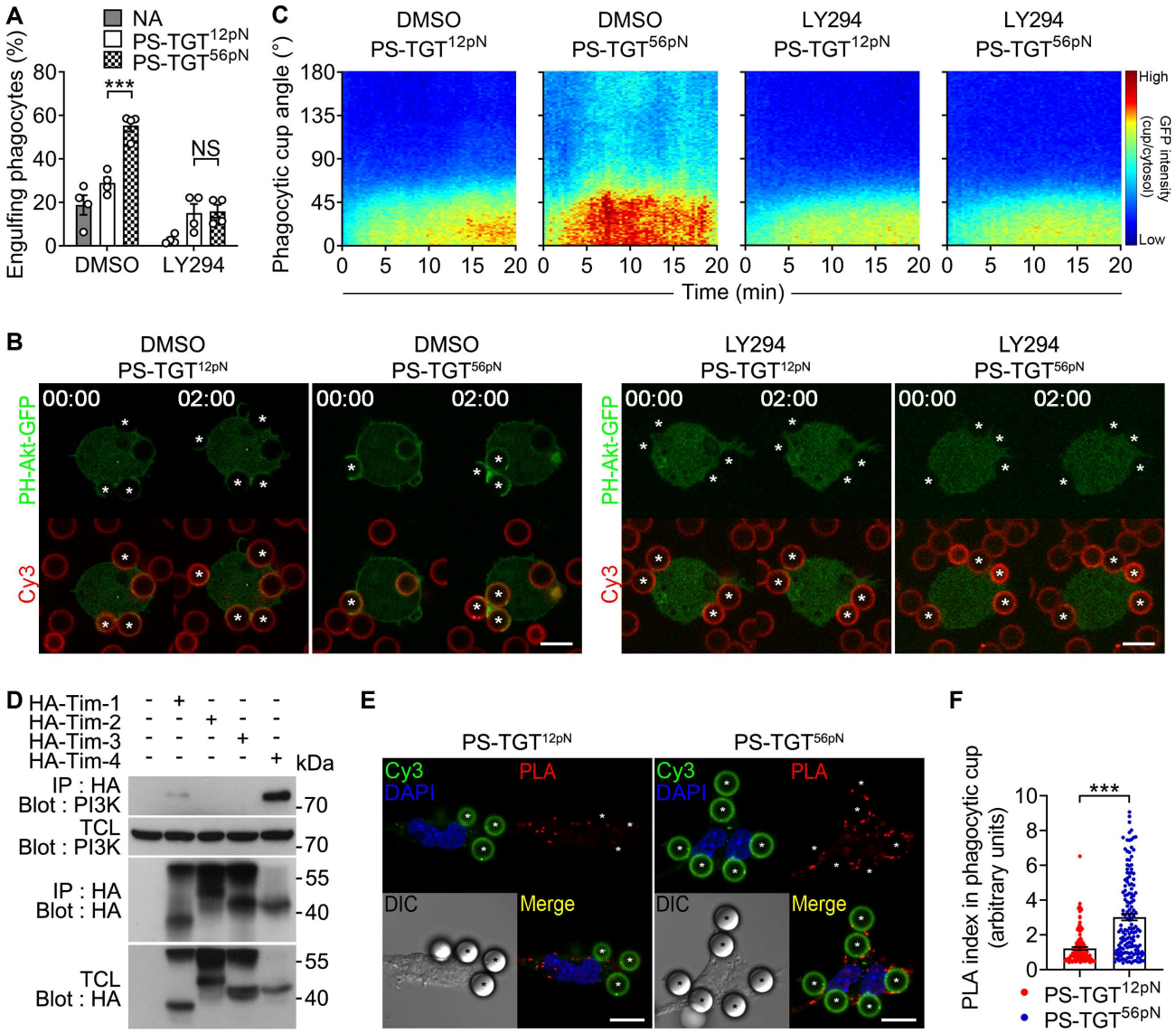
A
NA
PS-TGT12pN
PS-TGT56pN
Engulfing phagocytes (%)
80
60
40
20
0
***
NS
DMSO
LY294
C
DMSO PS-TGT12pN
DMSO PS-TGT56pN
LY294 PS-TGT12pN
LY294 PS-TGT56pN
Phagocytic cup angle (°)
180
135
90
45
0
0 5 10 15 20
Time (min)
High
GFP intensity (cup/cytosol)
Low
B
DMSO PS-TGT12pN
DMSO PS-TGT56pN
LY294 PS-TGT12pN
LY294 PS-TGT56pN
00:00
02:00
PH-Akt-GFP
Cy3
D
HA-Tim-1
HA-Tim-2
HA-Tim-3
HA-Tim-4
kDa
IP : HA
Blot : PI3K
TCL
Blot : PI3K
IP : HA
Blot : HA
TCL
Blot : HA
70
55
40
E
PS-TGT12pN
PS-TGT56pN
Cy3
DAPI
PLA
DIC
Merge
F
PLA index in phagocytic cup (arbitrary units)
10
8
6
4
2
0
***
PS-TGT12pN
PS-TGT56pN

486 **Fig. 3. The tension modulates PI3K activity.**

487 (**A**) J774A.1 cells pre-incubated with LY294 (LY294002, 50 μM) for 10 min were incubated with
488 the indicated Cy3-labeled beads and analyzed by flow cytometry. Data are mean ± s.e.m. from
489 n=4 independent experiments. ***P < 0.001; NS, not significant; two-way ANOVA. (**B** and **C**)
490 J774A.1 cells stably expressing PH-Akt-GFP were incubated with Cy3-labeled PS-TGT beads
491 for 30 min and observed by time-lapse confocal microscopy. Asterisks indicate beads with
492 extended phagocytic cups (B). The intensities of GFP at phagocytic cups were measured (C).
493 Scale bar, 10 μm. n=67 beads for PS-TGT^{12pN} (DMSO), n=41 beads for PS-TGT^{56pN} (DMSO),
494 n=70 beads for PS-TGT^{12pN} (LY294002), and n=54 beads for PS-TGT^{56pN} (LY294002). (**D**)
495 Lysates of 293T cells transfected with the indicated plasmids were incubated with anti-HA
496 antibody-conjugated agarose beads. Bead-bound proteins were detected by the indicated
497 antibodies. IP, immunoprecipitation; TCL, total cell lysate. (**E** and **F**) Peritoneal macrophages
498 were incubated with Cy3-labeled PS-TGT beads for 10 min, fixed, blocked, and incubated with
499 anti-Tim4 and anti-PI3K antibodies. Then, PLA probes were stained and incubated in
500 amplification solution. PLA signals were observed using confocal microscopy (E), and PLA
501 signals for each bead were quantified (F). Asterisks indicate beads with extended phagocytic
502 cups. Scale bar, 10 μm. Data are mean ± s.e.m. from n=126 beads for PS-TGT^{12pN} and n=153
503 beads for PS-TGT^{56pN}. ***P < 0.001; two-tailed unpaired Student's *t* test.

504

505

Figure 4

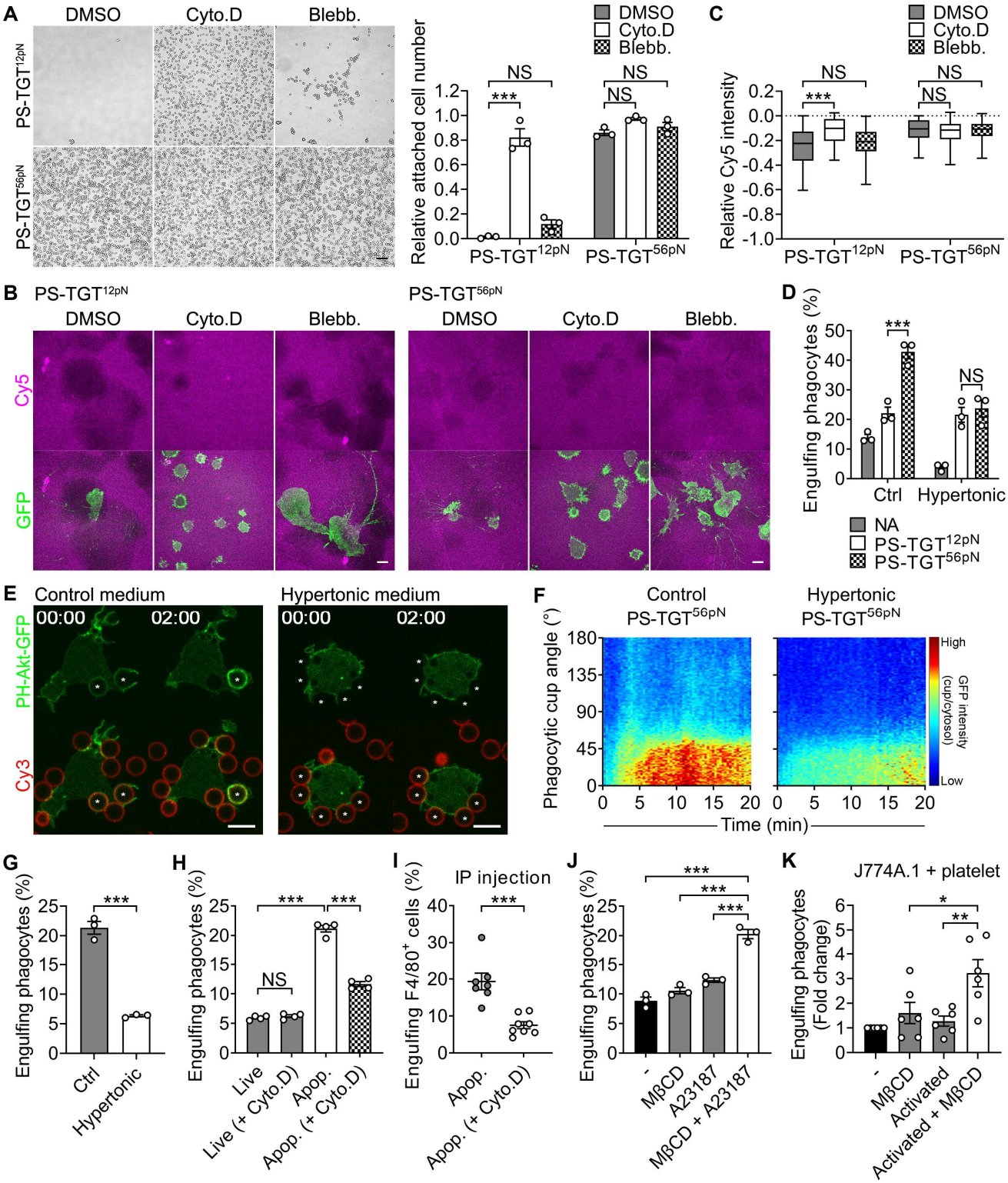
A
DMSO
Cyto.D
Blebb.
PS-TGT12pN
PS-TGT56pN
Relative attached cell number
NS
***
B
Cy5
GFP
C
Relative Cy5 intensity
D
Engulfing phagocytes (%)
Ctrl
Hypertonic
NA
E
Control medium
Hypertonic medium
PH-Akt-GFP
Cy3
00:00
02:00
F
Control
Hypertonic
Phagocytic cup angle (°)
Time (min)
High
Low
GFP intensity (cup/cytosol)
G
H
Live
Apop.
Live (+ Cyto.D)
Apop. (+ Cyto.D)
I
IP injection
Engulfing F4/80+ cells (%)
J
MβCD
A23187
MβCD + A23187
K
J774A.1 + platelet
Engulfing phagocytes (Fold change)
Activated
Activated + MβCD

506 **Fig. 4. Membrane tension increased by actin polymerization loads tension on PS-PSRs.**
507 (**A**) J774A.1 cells incubated on the indicated PS-TGT plates for 5 min were washed and then
508 further incubated in the absence or presence of cytochalasin D (1 μM) or blebbistatin (10 μM)
509 for 60 min. The cell number at 60 min relative to that at 5 min was calculated. Representative
510 images after incubation for 60 min are shown. Scale bar, 200 μm. Cyto.D, cytochalasin D;
511 Blebb, blebbistatin. Data are mean ± s.e.m. from n=3 independent experiments. ***P < 0.001;
512 NS, not significant; two-way ANOVA. (**B** and **C**) J774A.1 cells stably expressing membrane-
513 targeted GFP were incubated on the indicated PS-TGT plates for 60 min and Cy5 fluorescence
514 was observed by confocal microscopy (B). Relative Cy5 intensities were calculated. The
515 intensity of Cy5 in the area where cells were absent was set to 0 (C). Data are presented in the
516 box-and-whisker plot. n=55 cells for PS-TGT^{12pN} (DMSO), n=172 cells for PS-TGT^{12pN} (Cyto.D),
517 n=115 cells for PS-TGT^{12pN} (Blebb.), n=92 cells for PS-TGT^{56pN} (DMSO), n=189 cells for PS-
518 TGT^{56pN} (Cyto.D), and n=161 cells for PS-TGT^{56pN} (Blebb.). ***P < 0.001; NS, not significant;
519 two-way ANOVA. (**D**) J774A.1 cells pre-incubated in medium containing 150 mM sucrose
520 (hypertonic medium) were incubated with the indicated beads for 10 min and analyzed by flow
521 cytometry. Data are mean ± s.e.m. from n=3 independent experiments. ***P < 0.001; NS, not
522 significant; two-way ANOVA. (**E** and **F**) J774A.1 cells stably expressing PH-Akt-GFP were pre-
523 incubated in medium containing 150 mM sucrose and then incubated with Cy3-labeled PS-
524 TGT^{56pN} beads and observed by time-lapse confocal microscopy. Asterisks indicate beads with
525 extended phagocytic cups (E). The intensities of GFP fluorescence at phagocytic cups around
526 the beads were measured (F). Scale bar, 10 μm. n=40 beads for PS-TGT^{56pN} (control medium)
527 and n=51 beads for PS-TGT^{56pN} (hypertonic medium). (**G**) J774A.1 cells pre-incubated in
528 medium containing 150 mM sucrose were incubated with apoptotic Jurkat cells for 30 min and
529 analyzed by flow cytometry. Data are mean ± s.e.m. from n=3 independent experiments.
530 ***P < 0.001; two-tailed unpaired Student's *t* test. (**H**) J774A.1 cells were incubated with live or

531 apoptotic Jurkat cells treated with or without cytochalasin D (2 μM) for 30 min and analyzed by
532 flow cytometry. Data are mean ± s.e.m. from n=4 independent experiments. ***P < 0.001; NS,
533 not significant; one-way ANOVA. (**I**) TAMRA-stained apoptotic Jurkat cells treated with or without
534 cytochalasin D (2 μM) were intraperitoneally injected into 8-week-old mice. Peritoneal exudates
535 from the mice were stained with an anti-F4/80 antibody and analyzed by flow cytometry. Data
536 are mean ± s.e.m. from n=7 mice for Apop. and n=8 mice for Apop. (+Cyto.D). ***P < 0.001; two-
537 tailed unpaired Student's *t* test. (**J**) J774A.1 cells were incubated with Jurkat cells treated with
538 MβCD (1 mM), A23187 (10 μM), or MβCD and A23187 for 30 min and analyzed by flow
539 cytometry. Data are mean ± s.e.m. from n=3 independent experiments. ***P < 0.001; one-way
540 ANOVA. (**K**) J774A.1 cells were incubated with platelets treated with MβCD (10 mM) or
541 activated platelets treated with MβCD for 30 min and analyzed by flow cytometry. Data are
542 mean ± s.e.m. from n=6 independent experiments. *P < 0.05, **P < 0.01; one-way ANOVA.